Stark-effect studies in xenon autoionizing Rydberg states using a tunable extreme-ultraviolet laser source

W. E. Ernst,* T. P. Softley,† and R. N. Zare

Department of Chemistry, Stanford University, Stanford, California 94305

(Received 16 November 1987)

The Stark spectra of autoionizing Rydberg states of Xe converging to the second ionization limit $5p^5\,^2P_{1/2}$ have been investigated as a function of applied electric field over the range 26–2362 V/cm. Single-photon excitation from the Xe ground state was achieved using coherent radiation near 92.5 nm, generated by frequency tripling the pulsed output of a frequency-doubled dye laser in a free jet of rare-gas atoms. For the lowest electric field only the ns' and nd' series were observed. As the electric field was increased the np' series appeared because of the mixing of wave functions with different l values. Further increase of the electric field caused the appearance of hydrogenlike Stark manifolds. The Stark spectrum was simulated in a two-step procedure with no adjustable parameters. Using a jl-coupling basis set the Hamiltonian matrix was diagonalized to determine the energy levels and corresponding eigenfunctions for a given electric field strength. The intensities and line shapes were then calculated using the formalism developed by Fano for a many-discrete-level–single-continuum configuration interaction. This treatment was sufficient to reproduce the positions, widths, and shapes of most observed features. At field strengths between 1000 and 2000 V/cm, however, an additional modulation structure with a spacing of about 2.7 cm^{-1} appeared on top of the $|M|=1$ autoionizing resonances, which could not be explained by our simple theoretical model.

I. INTRODUCTION

The Rydberg spectra of the rare gases have been a matter of interest for both experimentalists and theorists for many years. Because of fine structure in the ionic core, two sets of singly excited Rydberg series converge to two separate ionization limits. The series converging to the upper $(j=\frac{1}{2})$ fine-structure level autoionizes. Strong interactions between both series can be observed, as is characteristic of heavy atoms.

Among the heavy rare gases, xenon Rydberg series have been investigated by several research groups using different experimental techniques. The earliest method used for the study of the rare-gas Rydberg spectra was classical vacuum-ultraviolet (vuv) absorption spectroscopy.[1] It was not until 1985, however, that a high-resoluton absorption spectrum of Xe was reported by Yoshino and Freeman[2] for the wavelength region 92.2–129.6 nm. Using a 6.65-m vacuum spectrograph they investigated the ns and nd Rydberg series converging to the first ionization limit as well as the autoionizing series ns' and nd'. They derived absolute term values for Rydberg states up to $n=66$ at an accuracy better than 0.2 cm^{-1}. This yielded precise values for the ionization energies. The application of multichannel quantum-defect theory (MQDT) (Ref. 3) was necessary for a correct description of the absorption spectrum.

Laser spectroscopy can provide very high resolution but is usually restricted to much longer wavelengths. In the case of rare-gas studies, metastable states were usually excited by electron impact in a first step. Rydberg states were then reached by subsequent absorption of one or two photons from visible or uv lasers. The total accuracy in determining Rydberg energies is gain on the order 0.2 cm^{-1}. Stebbings et al.[4] applied this method to a beam of Xe atoms. Grandin and Husson[5] studied Xe Rydberg states in a discharge cell with the same excitation scheme, and more recently Knight and Wang[6-8] performed extended laser-spectroscopic investigations on a beam of metastable Xe atoms. By choosing different intermediate levels, Rydbeg series of both even and odd parity could be observed.[4-8]

Single-photon laser excitation from the Xe ground state into Rydberg levels requires a vuv laser source. In the case of the autoionizing series, it is necessary to work in the windowless region below 104 nm, the extreme ultraviolet (xuv). Tunable coherent radiation in this part of the spectrum can be generated by frequency upconversion of a high-power dye laser.[9] Bonin, McIllrath, and Yoshino[10] used two-photon resonant frequency mixing of pulsed visible and uv laser radiation in Kr to study autoionizing resonance lines of Xe between 94.2 and 92.3 nm. Their xuv source provided 5×10^9 photons per pulse at a linewidth of 0.3 cm^{-1}. The accuracy in determining absolute term energies was comparable to that of Yoshino and Freeman.[2] As pointed out by Bonin et al., the resolution can be greatly improved by using fundamental laser radiation with a narrower linewidth. Compared to the classical technique, the smaller tuning range remains the major limitation of this type of xuv laser source. In principle, synchroton facilities can provide tunability all over the vuv and xuv. Unfortunately, in most cases the resolution is very limited and needs to be improved in the future by using better monochromators. In

a study of the Stark effect on Xe autoionizing resonances, Cole et al.[11] had only a resolution of about 50 cm^{-1}.

In spite of their limited resolution, Cole et al.[11] made the first observation of the mixing of optically allowed Rydberg series with the neighboring states of opposite parity at electric field strengths between 1 and 8 kV/cm. By applying laser spectroscopy to a beam of metastable Kr atoms in an external electric field (1–3 kV/cm), Delsart and Keller[12] performed the first high-resolution studies of the Stark effect on the autoionizing Rydberg series of a rare gas. Recently, Knight and Wang[13] used the same method to measure the Stark structure for the bound Rydberg states of Xe. They also observed a Stark-induced 6s-6d transition[14] which is forbidden at zero field.

We have chosen to study the Stark effect of autoionizing Rydberg states of Xe by one-photon excitation from the ground state using a tunable coherent xuv source. xuv radiation around 92.5 nm was generated by tripling the frequency of a frequency-doubled dye laser in a pulsed free jet of rare-gas atoms.[15] The xuv light was focused into a pulsed Xe beam. An external electric field of 26 to 2362 V/cm was applied to the interaction region. The linear polarization of the xuv radiation could be chosen to be parallel or perpendicular to the Stark field direction, thus exciting $M = 0$ or $|M| = 1$ levels, respectively. At zero field, only ns' and nd' Rydberg series can be observed. However, an electric field strength of 150 V/cm is sufficient to mix states of opposite parity, allowing us to observe the np' series. Systematic measurements allowed the determination of energy levels for the np' series in the range $18 \leq n \leq 31$ by extrapolating to zero field. Furthermore, we studied the electric field dependence of the line shifts and splittings as well as the field behavior of hydrogenlike Stark manifolds. A simple model is introduced in Sec. IV for the calculation of the Stark effect. In this model we employ a jl-coupling scheme and diagonalize the Stark Hamiltonian. The interaction of the derived eigenfunctions with a single continuum can explain most of the observed features. However, this treatment is unable to account for the observation of an additional modulation structure in the photoionization cross section as a function of energy at field strengths around 1 kV/cm.

II. EXPERIMENT

Figure 1 shows a schematic diagram of the experimental apparatus. A detailed description of our xuv laser spectrometer has been given elsewhere.[16] The light from a pulsed Nd:YAG (where YAG stands for yttrium aluminum garnet) pumped dye laser operated with Rhodamine 590 is frequency doubled in a KDP (potassium dihydrogen phospate) crystal. Without the use of an intracavity etalon, the linewidth of the dye laser is about 0.5 cm^{-1}. The uv pulse (~ 10 mJ energy and ~ 6 ns duration) is focused into a pulsed free jet of argon or xenon which serves as a gaseous nonlinear medium.[15] Frequency tripling in a Xe jet yields about 2×10^8 photons per pulse in the 93-nm region, while the conversion efficiency in Ar is about one order of magnitude smaller. There is a slight
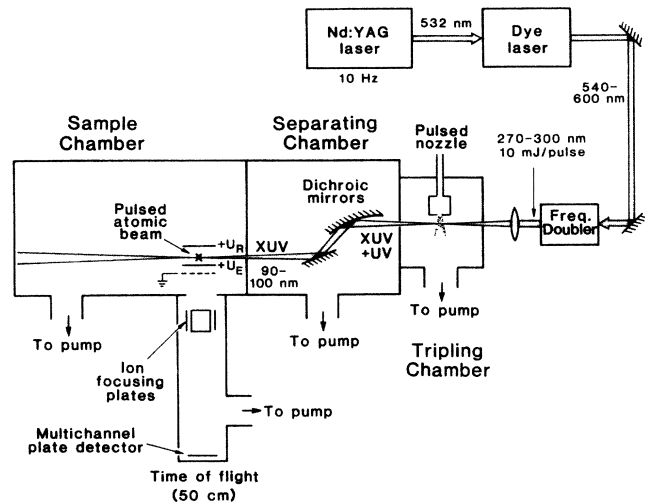

FIG. 1. Experimental setup.

amount of absorption of the generated xuv in the Xe jet which can be minimized by adjusting the uv focus in the beam. With careful alignment, the xuv tuning curve shows only small variations in power caused by these absorption features. After the jet, the xuv is separated from the $\sim 10^6$ more intense uv fundamental radiation by using two dichroic beam splitters.[16,17] This separation is needed for the investigation of samples for which the xuv spectroscopy might be obscured by uv multiphoton processes. There is no danger of such processes in the rare gases at the applied uv power, but the beam-splitter setup has an additional feature which makes it attractive even in the study of a rare gas. One of the xuv reflecting surfaces has a geometry for focusing the xuv into the sample with a round spot size of less than 1 mm in diameter.[16]

In this study the sample is a pulsed Xe beam injected between a pair of metal plates serving as ion repeller and extractor plates of a time-of-flight mass spectrometer and also as Stark plates in the electric field studies (see Fig. 1). Xenon atoms excited by the xuv into Rydberg states between the two ionization limits autoionize. The resulting ions are sent through a slit in the extractor plate into a 50-cm time-of-flight mass spectrometer. The sharp focus of the xuv light permits an excellent mass resolution. A minimum potential difference of 50 V between the repeller and extractor plates, corresponding to a field strength of 26 V/cm, is required to obtain a good ion signal. The potential difference can be increased to 4500 V (2362 V/cm) in the present setup. The voltages are applied continuously, hence there is always a finite electric field present in the interaction region.

The electric field and time-of-flight arrangement could be rotated by 90° with respect to the laser light polarization. In this way the field could be chosen parallel or perpendicular to the laser polarization, allowing to the excitation into Rydberg states with the selection rules $\Delta M = 0$ or $\Delta M \pm 1$, respectively.

The autoionizing Rydberg series were recorded by monitoring the Xe ion signal in the wavelength range from 92.8 to 92.3 nm at a resoluton of 1.2 cm^{-1}. As an

absolute wavelength calibration, we used the zero-field line positions of the ns' series tabulated in Ref. 2. A spectrum was obtained separately for eight different field strengths in the range given above. In general, xenon was used as the tripling gas, as this gave the better signal to noise ratio compared to argon. When argon is used, the spectrum appears the same but the intensities are slightly different caused by the wavelength-dependent xuv absorption in the Xe tripling gas. As a consequence, Xe should not be used as a tripling gas in this wavelength range when intensities or linewidths are to be determined to high accuracy.

III. RESULTS AND DISCUSSION

Figure 2 shows a part of the observed Rydberg spectrum for different electric field strengths. The depicted scans were recorded with perpendicular polarization using ten-shot signal averaging which corresponds to a time constant of 1 s. We will discuss several features which are apparent in this figure.

A. Observation of the np' series and the nd' $J = 2$ series

The lowest trace (26 V/cm) shows only the narrow ns' and broad nd' resonances and is virtually identical to the absorption spectrum recorded at zero field by Yoshino and Freeman.[2] At 787 V/cm (2nd trace) two new series of lines can be observed. One of these is labeled in the figure as np', while the second set of lines, observed to slightly shorter wavelength, is a fine-structure component of the nd' series having total angular momentum $J = 2$. The basis for our identification will be discussed subsequently. The intensities of the new series increase with principal quantum number and field strength. The np' transitions are parity forbidden at zero field but become allowed because the field mixes wave functions of opposite parity with different l. Electric-field-induced transitions into np' levels were also observed for krypton by Delsart and Keller.[12] The transition to the nd' $J = 2$ series from the ground state $(J = 0)$ is also forbidden in zero field; the intensity mechanism in the presence of a field is discussed in Sec. IV.
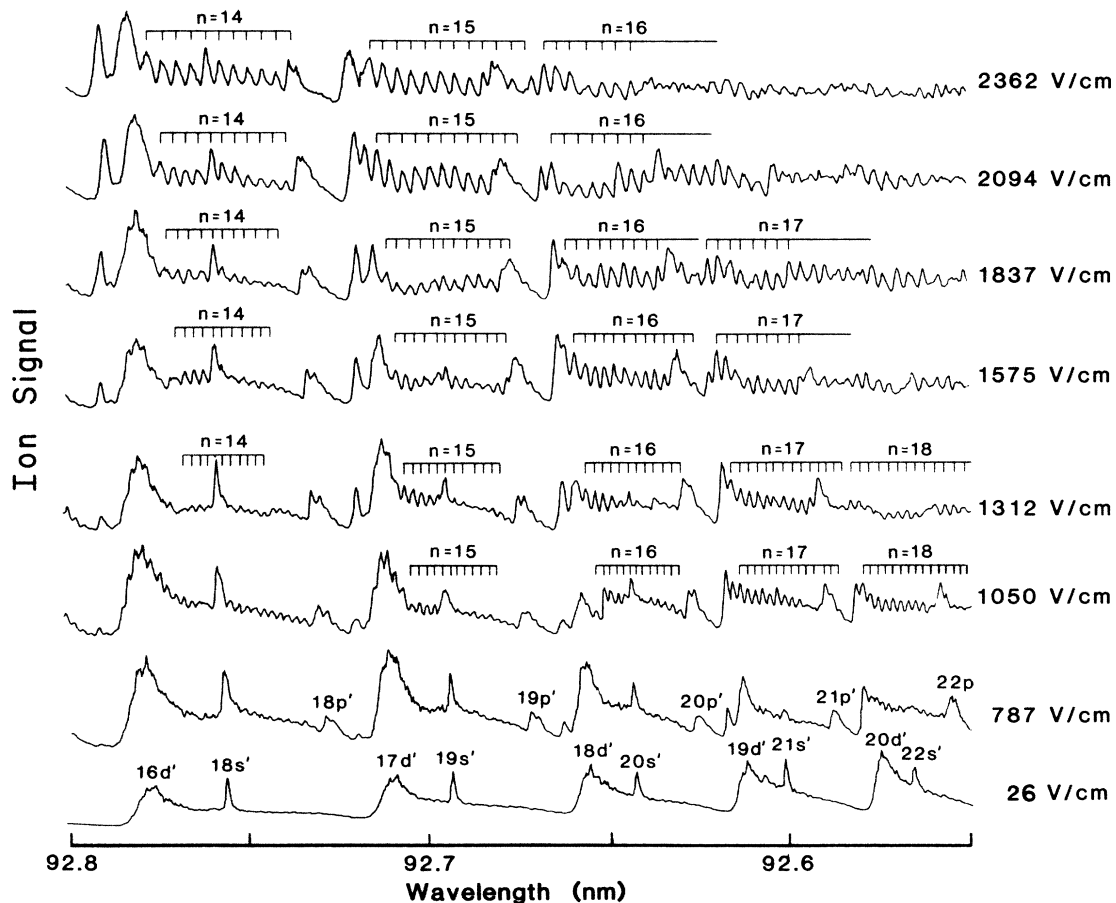

FIG. 2. Measured Stark spectrum of Xe autoionizing Rydberg states in the wavelength range from 92.8 to 92.55 nm for various electric field strengths and excitation into states with $|M| = 1$.

B. Hydrogenlike Stark manifolds

At Stark fields above 1000 V/cm the mixing of l states with negligible quantum defect ($l = 3$ to $n - 1$) causes the appearance of hydrogenlike Stark manifolds in the wavelength region depicted in Fig. 2. In the range between 1000 and 2000 V/cm these manifolds consist of $n - 3$ members because the ns', np', and nd' levels have a larger quantum defect and are well separated from the degenerate sets. At higher field strengths, the ns' lines disappear first in the manifold, as seen in Fig. 2. Finally, the manifolds reach the p',d' complexes, leading to a situation with fully developed hydrogenlike behavior. Figure 3 gives an overview of the energy dependence of the $|M| = 1$ components on the electric field strength E. Marked on the electric field axis is the value $E = 1/(3n^5)$ for $n = 15$. At this field strength the first anticrossing between the $n = 15$ and $n = 16$ manifolds is predicted to occur,[18] in good agreement with the observations. We measured the splittings $\delta\sigma$ between the Stark-manifold components at different field strengths and plotted them versus n in Fig. 4 with logarithmic scales. The slopes are 0.68 for 2100 V/cm, 0.65 for 1837 V/cm, and 0.70 for 1312 V/cm. These results seem to agree with the $n^{0.7}$ dependence of the splittings, which was seen by Delsart and Keller[12] in the case of Kr. For the highest fields and principal quantum numbers studied (i.e., the top right-hand corner of Fig. 2), the manifolds corresponding to different principal quantum numbers interact strongly, giving a very complex structure in the spectrum.

C. Polarization dependence in the spectra of p', d' complexes

By changing the laser polarization direction with respect to the Stark field, we recorded spectra with the selection rules $\Delta M = 0$ and $\Delta M = \pm 1$, corresponding to an excitation from the ground state into Rydberg states with $M = 0$ and $|M| = 1$, respectively. Delsart and Keller[12] investigated the Stark effect in Kr autoionizing Rydberg series with the use of two-step laser excitation from a metastable state. They reported no appreciable change of the spectra with laser polarization. In their Stark-effect studies of bound Rydberg states of Xe, Knight and Wang[13] did not find a difference in their plotted Stark maps for $M = 0$ and $|M| = 1$. The spectra in Fig. 2 show our recordings for $|M| = 1$. In contrast to the observations in Refs. 12 and 13, we found a considerable difference in the mixing of states with different l for $M = 0$ and $|M| = 1$. In Fig. 5 we show a part of the spectrum near the $17d'$ line for a Stark field of 1575 V/cm for both $M = 0$ and $|M| = 1$. For $|M| = 0$ only one new series is observed in addition to the manifold lines; the nd' $J = 2$ series, observed for $|M| = 1$, does not appear, while the np' series is shifted with respect to the $|M| = 1$ np' line positions. We anticipate the results of the calculations presented subsequently in stating that different fine-structure components of the np' series are observed in the two different polarizations, accounting for the apparent shift. For $M = 0$ the observed component has total angular momentum $J = 0$ and may be represented in jl-coupling notation as $np'[1/2]_0$. The np' series observed for $|M| = 1$ is shown later to be an un-

resolved superposition of $J = 1$ and $J = 2$ components. The $J = 0$ series has not been observed previously and in Table I we list our experimentally determined energy levels for this component from $n = 18$ to $n = 31$ These energies were obtained by recording the line positions for several different electric field strengths in the range 80–630 V/cm and then extrapolating to zero field. The absolute accuracy is ± 1 cm^{-1} and we determine a quantum defect of $\delta = 3.50$.

There is no measurable difference in the manifold splittings for $M = 0$ compared to $|M| = 1$. Nevertheless, it is apparent from Fig. 5 that the manifold lines are more intense for $M = 0$ relative to the $17d'$ line suggesting that the nd' series is more strongly mixed with the manifold levels.

D. Oscillations superimposed on the autoionizing resonances

Figure 2 shows even more resonances in the intermediate field strength region between 1000 and 2000 V/cm at energies lying between the manifolds. A fairly strong modulation is apparent over the complete wavelength range, but particularly at the long-wavelength end of the 1050-V/cm spectrum. The modulation is about 15% of the total ion yield and the distance between adjacent peaks is 2.7 cm^{-1}. The structure is superimposed on the normal autoionizing resonances and starts to be observed at 787 V/cm. Above 2000 V/cm, the hydrogenlike mani-
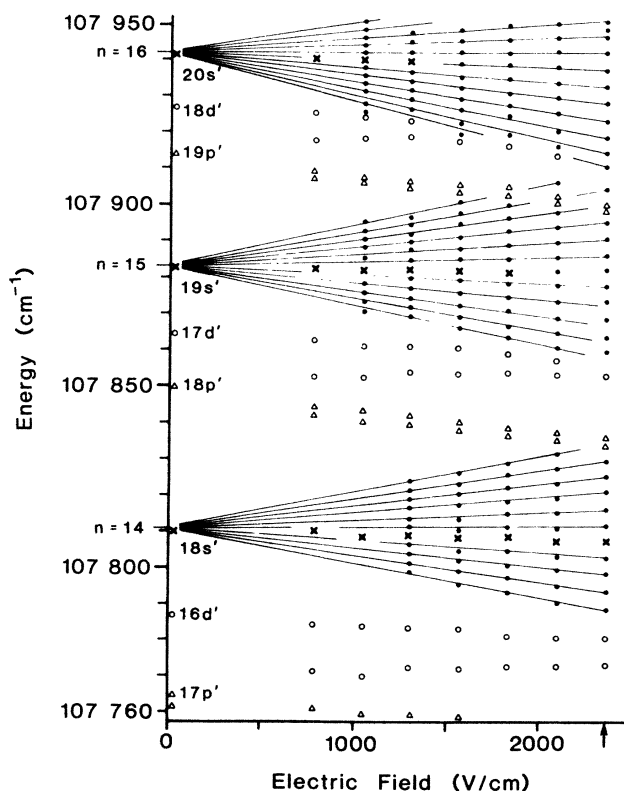
FIG. 3. Stark map for $|M| = 1$ in the region between the $n = 14$ and 16 manifolds (from experiment). The arrow on the electric field axis shows the value $E = 1/(3n^5)$ for $n = 15$.
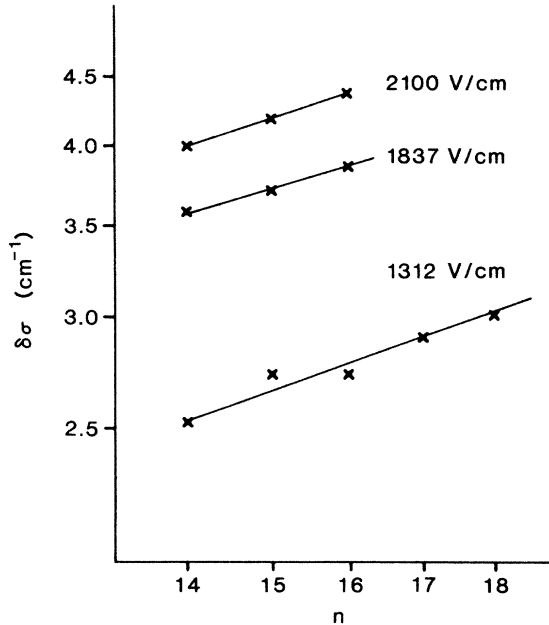
FIG. 4. Plot of the measured spacing between members of the Stark manifolds vs n with logarithmic scales for three electric field strengths. The slopes are 0.68, 0.65, 0.70 for 2100, 1837, and 1312 V/cm, respectively.
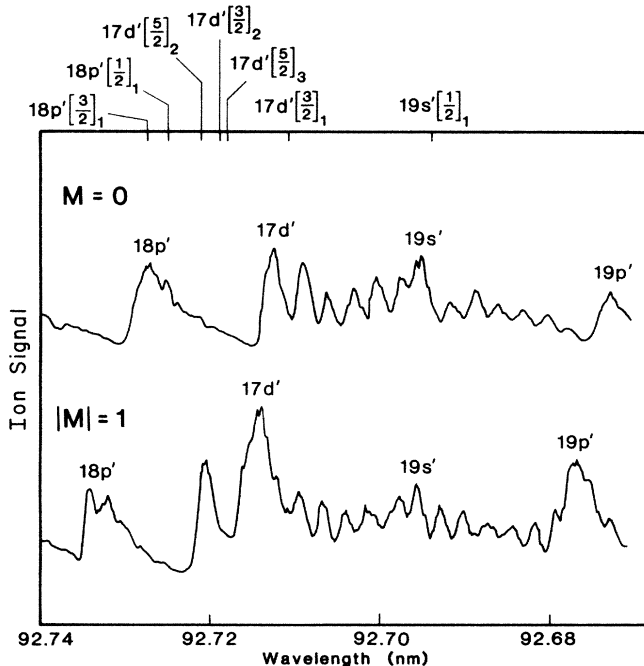

FIG. 5. Part of the measured Stark spectrum in the vicinity of the $19s'$ line for 1575 V/cm and excitation into states with $M=0$ (upper trace) and $|M|=1$ (lower trace). At this field strength the $n=15$ manifold covers the region between the $17d'$ and $19p'$ lines. Along the wavelength axis the zero-field positions of lines are given which are mixed by the Stark field (positions from Refs. 2, 7, 8, or according to Table II).

TABLE I. Derived energy values and effective quantum numbers for the np' $(J=0)$ levels from extrapolation to zero electric field.

n	Energy (cm^{-1}) $np'[\frac{1}{2}]_0$	n^* $np'[\frac{1}{2}]_0$
18	107 849.7	14.51
19	107 914.0	15.50
20	107 967.7	16.50
21	108 012.7	17.51
22	108 050.1	18.50
23	108 082.4	19.51
24	108 109.6	20.50
25	108 133.4	21.50
26	108 154.4	22.52
27	108 171.6	23.47
28	108 188.0	24.50
29	108 201.2	25.44
30	108 214.9	26.53
31	108 225.8	27.51

folds become dominant in intensity and the oscillations are no longer observed. In our measurements we found the regular structure only for $|M|=1$, but not for $M=0$. The 2.7-cm^{-1} spacing of the peaks corresponds to a frequency of about 100 GHz. To our knowledge no resonances of this kind have been observed previously in the rare-gas Rydberg spectrum near the second ionization limit.

Freeman and Economou[19] measured the electric field dependence of the photoionization cross section of Rb near threshold. They found a wavelength-dependent resonance structure that changes with the strength of the electric field. Sandner, Safinya, and Gallagher[20] made similar observations for Ba and Na. Both groups saw the structure only for $M=0$ but not for $|M|=1$. They interpret their results in terms of strong-field mixing near the ionization threshold for a Coulomb plus electric field potential. In the region immediately above the first ionization limit of Kr. Glab, Hillard, and Nayfeh[21] observed an electric-field-induced resonance riding on an autoionizing resonance. As in Refs. 19 and 20, the oscillations were found only for $M=0$ and corresponded to a much lower frequency than those in our spectra. Our observations were made in the region of 400 to 500 cm^{-1} below the second ionization limit and also below the classical field ionization limit.

IV. SIMULATION OF THE STARK SPECTRUM AND CONCLUSIONS

In this section we present a simulation of the xenon Stark spectrum which was used as a basis for identification of the observed features and also to further our understanding of the bound-continuum interactions in the xenon atom. The Rydberg spectra of the rare gases have long been a stimulus for advances in the theoretical understanding of many-electron atoms. To date, howev-

er, there appear to have been no calculations for the effect of electric fields on the autoionizing Rydberg series. A particular difficulty of any theoretical treatment is that, even at zero field, there is more than one autoionization channel accessible to a given Rydberg level, and when an electric field is present even more channels become available. In principle, therefore, we need to solve a complex multichannel problem. Based on the multichannel quantum-defect theory (MQDT) and WKB method, Harmin[22] performed calculations of the hydrogenic Stark effect and subsequently extended his theoretical treatment to nonhydrogenic Stark spectra,[23,24] especially for alkali-metal Rydberg states. Harmin's theory which was restricted to closed-shell ion cores was extended by Sakimoto[25] to the general case where the ion core is in an arbitrary state. References 22–25 show that the MQDT would be expected to provide the right tool for calculating the Stark effect of the Xe Rydberg series. However, such a treatment is involved, and we explore here a more simple approach.

Kelleher[26] has outlined how to calculate the widths, shapes, and shifts of autoionizing resonances by extending Fano's bound-continuum configuration-interaction treatment[27] to the many-continuum–many-discrete-state situation. However, in contrast to the single-continuum case, no simple analytical expression for the photoionization cross section as a function of energy was derived. The application of Kelleher's formalism requires the solution of a large set of coupled equations for each value of the energy.

Our treatment is in the same spirit as that of Kelleher but for the specific case of the xenon Rydberg series we are able to make a number of simplifications leading to a relatively straightforward and inexpensive calculation. We first assume that the positions of the autoionizing levels in the presence of a field are determined only by the Stark mixing with the set of discrete $j = \frac{1}{2}$ Rydberg states. We further assume that there is no field-induced mixing of the continuum states ($j = \frac{3}{2}$). Our most important approximation is to suppose that the autoionization of the mixed eigenstates of the Stark Hamiltonian occurs through no more than two channels; indeed, we show in this section that most of the spectral features can be ex-

plained by using just one channel.

In the first step we diagonalize the Stark energy matrix for the discrete Rydberg states ignoring any bound-continuum interactions, using the known energy positions of the interacting levels. For the moderate electric fields of the experiment, l mixing within an n manifold is dominant, thus reducing the size of the basis set which must be used. We follow the procedure of Knight and Wang,[13] who in their study of the Stark effect of the bound Xe Rydberg state ($j = \frac{3}{2}$) set up the total energy matrix in a jl-coupling basis set. The Rydberg electron orbital angular momentum l is strongly coupled to the total angular momentum j of the ion core yielding an angular momentum $\mathbf{K} = \mathbf{j} + \mathbf{l}$. Then $\mathbf{K}$ is weakly coupled to the Rydberg electron spin s producing the total angular momentum $\mathbf{J} = \mathbf{K} + \mathbf{s}$. The basis functions are written as $nl[K]_J$. A prime on l indicates $j = \frac{1}{2}$. For $j = \frac{1}{2}$ we get $K = l' \pm \frac{1}{2}$ and $J = K \pm \frac{1}{2}$, i.e., four basis functions for each l except for ns' and np'. We use the Hamiltonian $H = H_0 + H_{\text{Stark}}$ with $H_{\text{Stark}} = eEz$ and diagonalize the matrix separately for $M = 0$ and $|M| = 1$. Note that the $M = 0$ Stark Hamiltonian is of higher rank than the $|M| = 1$ Hamiltonian because basis states with $J = 0$ do not exist in the latter case.

The diagonal matrix elements are given by the experimentally determined zero-field energy levels. Although these are not exactly the energies of the pure $j = \frac{1}{2}$ states due to a contribution from the $j = \frac{1}{2} \leftrightarrow j = \frac{3}{2}$ mixing, we assume that this energy shift is small and uses values, the derivation of which are described in Table II.

For the computation of the off-diagonal matrix elements of the Stark Hamiltonian we proceed as described in Ref. 13. The selection rules in jl coupling are

$$\Delta M = \Delta s = \Delta j = 0 \; ,$$

$$\Delta J = 0, \pm 1 \text{ for } |M| = 1 \text{ and } \Delta J = \pm 1 \text{ for } M = 0 \; ,$$

$$\Delta K = 0, \pm 1 \; , \tag{1}$$

$$\Delta l = \pm 1 \; .$$

Defining v as the effective quantum number and using the standard angular momentum algebra as was used in Ref. 13, we get the matrix elements

$$\langle (vlj)KsJM \,|\, z \,|\, (v'l'j)K'sJ'M \rangle = (-1)^{J+J'+K+K'+l+j+s-M}[(2J+1)(2J'+1)(2K+1)(2K'+1)]^{1/2}$$

$$\times \begin{bmatrix} J & 1 & J' \\ -M & 0 & M \end{bmatrix} \begin{Bmatrix} K & J & s \\ J' & K' & 1 \end{Bmatrix} \begin{Bmatrix} l & K & j \\ K' & l' & 1 \end{Bmatrix} \langle vl \| r \| v'l' \rangle \; , \tag{2}$$

with

$$\langle vl \| r \| v'l' \rangle = \begin{cases} -\sqrt{l+1} \langle vl \,|\, r \,|\, v'l+1 \rangle, & l' = l+1 \\ \sqrt{l} \langle vl \,|\, r \,|\, v'l-1 \rangle, & l' = l-1. \end{cases} \tag{3}$$

The radial integrals are evaluated in the Coulomb approximation using the formalism of Edmonds et al.,[28]

$$\langle vl \,|\, r \,|\, v'l' \rangle = \{ \tfrac{3}{2} v_c^2 [1 - (l_c/v_c)^2]^{1/2} \} \sum_{p=0}^{3} \gamma^p g_p(s) \; , \tag{4}$$

with $l_c = \max(l, l')$.

$$v_c = 2/(1/v + 1/v') \; ,$$

$$s = v - v' \; ,$$

$$\gamma = \Delta l (l_c / v_c) \; ,$$

$$\Delta l = l' - l \; .$$

The functions $g_p(s)$ are tabulated in Ref. 28. Linear in-

TABLE II. Origin of the zero-field energy values of $nl'[K]_j$ basis states used in the Stark-effect calculation (δ=quantum defect of the Rydberg series).

State	Source for energy levels
$ns'[\frac{1}{2}]_0$	Up to $n=15$ given in Ref. 7; for $n \geq 16$, constant $\delta=4.02$ assumed
$ns'[\frac{1}{2}]_1$	Given in Ref. 7
$np'[\frac{1}{2}]_0$	This work, from zero-field extrapolation; see Sec. IV, constant $\delta=3.50$
$np'[\frac{1}{2}]_1$	Up to $n=17$ given in Ref. 8; for $n \geq 18$. constant $\delta=3.548$ assumed
$np'[\frac{3}{2}]_1$	Up to $n=17$ given in Ref. 8; for $n \geq 18$, constant $\delta=3.581$ assumed
$np'[\frac{3}{2}]_2$	Not known, based on the relative ordering of fine-structure components for the nd' series constant $\delta=3.56$
nd'	Given in Ref. 7
nf'	Not known; constant $\delta=0.055$ assumed, which is the value for the nf $(j=\frac{3}{2})$ series given in Ref. 6
$nl'(l'>3)$	Not known, constant $\delta=0$ assumed

terpolation was applied for s values between the listed ones.

For describing the energy levels in the range 92.8–92.55 nm, corresponding to principal quantum numbers $\nu=13.4$–18.5, all basis functions with $\nu=12.4$–20.6 were included in the calculation. This amounts to a total number of 552 basis functions for $M=0$ and 535 for $|M|=1$. In order to save computer time and storage space, the total spectral range was split into four overlapping segments for which only the diagonalization of matrices of about rank 300 was needed. For example, it was sufficient to use a set of 328 basis functions for the range 92.75–92.65 nm displayed in Fig. 5.

For a given electric field strength eigenvalues and eigenfunctions were determined. In the subsequent discussion we represent the jl-coupling basis functions using the notation ϕ_{ni}, where n is the principal quantum number and i represents a particular set of values for l, K, and J. The mth eigenfunction of the Stark Hamiltonian may therefore be written

$$\Phi_m = \sum_i \sum_n C_{im}^n \phi_{ni} .$$ (5)

The transition moment from the ground state to the state m is given by

$$\langle \Phi_m | T | \psi_0 \rangle = \sum_i \sum_n C_{im}^n \langle \phi_{ni} | T | \psi_0 \rangle$$ (6)

where T is the transition-moment operator and the $\langle \phi_{ni} | T | \psi_0 \rangle$ are the zero-field transition moments. The only contributions to the summation in (6) will be from the $nd'[\frac{3}{2}]_1$ and the $ns'[\frac{1}{2}]_1$ series. The nd' lines have considerably greater zero-field intensity than the ns' lines and in the most simple treatment used below we chose to

ignore the contribution to the intensities from the ns' transition.

A full simulation requires a calculation of linewidths and shapes in addition to the intensities; hence the coupling of the $j=\frac{1}{2}$ states to the $j=\frac{3}{2}$ continuum states must be considered. We assume that the $j=\frac{3}{2}$ continua are unperturbed by the electric field and note that there is no additional mixing of the $j=\frac{1}{2}$ and $j=\frac{3}{2}$ states caused by the H_{Stark} part of the Hamiltonian. In this case the mixing of the discrete states should result in a redistribution of linewidth similar to the redistribution of intensity in Eq. (6). If we further assume that each series of states i is coupled to just a single continuum and that each continuum state $X_i(E)$ is unique to the series i, then the linewidth for a transition to level m is given by

$$\frac{\Gamma_m}{2\pi} = \sum_i \left| \sum_n C_{im}^n V_{ni} \right|^2 ,$$ (7)

where $V_{ni} = \langle \phi_{ni} | V | X_i(E) \rangle$ and V is that part of the H_0 which is responsible for bound-continuum coupling. The magnitude of V_{ni} can be deduced from the zero-field linewidths Γ_{ni} by using the Fermi golden rule expression,

$$\Gamma_{ni} = 2\pi | V_{ni} |^2 .$$ (8)

Wang and Knight measured approximate autoionization linewidths for the ns' and nd' series, which we list in Table III. The linewidths for np' and nf' and higher series are not known, but we assume that they are smaller than for nd', which is fairly certain for $l'>2$. We note here that the linewidths are largest for $nd'[\frac{3}{2}]_1$ and on that basis we make a major simplification; we assume that the coupling of the $nd'[\frac{3}{2}]_1$ states to the continuum makes the major contribution in Eq. (7) and, therefore, we set all other linewidth contributions to zero. Hence

TABLE III. Autoionization rates Γ for the ns' and nd' Rydberg series as given by Wang and Knight (Ref. 7) with an error of $\pm 30\%$. n^* is the effective quantum number.

Rydberg series	Γ (cm^{-1})
$ns'[\frac{1}{2}]_0$	$1400/n^{*3}$
$ns'[\frac{1}{2}]_1$	$1300/n^{*3}$
$nd'[\frac{3}{2}]_1$	$35000/n^{*3}$
$nd'[\frac{3}{2}]_2$	$12000/n^{*3}$
$nd'[\frac{5}{2}]_2$	$4000/n^{*3}$
$nd'[\frac{5}{2}]_3$	$6000/n^{*3}$

$$\Gamma_m^i = 2\pi \left| \sum_n C_{im}^n V_{ni} \right|^2 , \tag{9}$$

where $i \equiv d[\frac{3}{2}]_1$. As all the $nd'[\frac{3}{2}]_1$ levels interact with the same continuum, we have reduced the problem to the

interaction of many discrete levels with a single continuum. We can then apply Fano's formalism[27] for the total photoionization cross section of an autoionizing resonance as a function of the energy E:

$$\sigma^i(E) = \sigma_0^i \cos^2 \Delta^i \left[\sum_m q_m^i \tan\Delta_m^i - 1 \right]^2 . \tag{10}$$

The summation is over the discrete levels m and we have retained the superscript i to indicate that only the autoionization channel is being considered.

σ_0^i is the direct photoionization cross section for channel i,

$$\tan\Delta_m^i = \Gamma_m^i / [2(E - E_m)] , \tag{11}$$

$$\tan\Delta^i = \sum_m q_m^i \tan\Delta_m^i , \tag{12}$$

and

$$q_m^i = \frac{\langle \phi_{ni} | T | \psi_0 \rangle + P \int V_{ni}(E') \langle \chi_i(E') | T | \psi_0 \rangle / (E - E') dE'}{\pi V_{ni}(E) \langle \chi_i(E) | T | \psi_0 \rangle} , \tag{13}$$

where

$$V_{mi}(E) = \sum_n C_{im}^n V_{ni}(E) , \tag{14}$$

$$\langle \Phi_m | T | \psi_0 \rangle = \sum_n C_{im}^n \langle \phi_{ni} | T | \psi_0 \rangle , \tag{15}$$

and P means "integrate over the principal part of." Note

that in Eqs. (9), (14), and (15) we consider explicitly the possibility that more than one member of the series i is mixed into a given eigenfunction Φ_m. For most levels, however, only one member will be important; in that case the summation signs disappear and combining (14) and (15) with (13), the C_{im}^n's cancel and we are left with

$$q_m^i = \frac{\langle \phi_{ni} | T | \psi_0 \rangle + P \int V_{ni}(E') \langle \chi_i(E') | T | \psi_0 \rangle / (E - E') dE'}{\pi V_{ni}(E) \langle \chi_i(E) | T | \psi_0 \rangle} , \tag{16}$$

which is simply the q value for the zero-field state ϕ_{ni}. Here m is used to represent eigenfunctions of the Stark Hamiltonian, while n is used to represent the zero-field basis states. The equality (16) remains as a good approximation, even if more than one member of the $nd'[\frac{3}{2}]_1$ series contributes to the eigenfunction because the various matrix elements in (16) vary only slowly between adjacent members of the series. (q_n^i is generally a constant for any series.)

It is important to note that if we use approximation (16), then all the input parameters for the simulation can be determined from the zero-field spectroscopy, that is, there are no adjustable parameters. For a comparison with experimental Stark spectra, the calculated photoionization cross section was convoluted with a 1.2-cm^{-1} instrumental linewidth.

The results of our calculations performed for the same electric field strengths as used experimentally are plotted in Fig. 6. We emphasize again that the results were obtained assuming that the zero-field transition from the

ground state to the $nd'[\frac{3}{2}]_1$ series is the source of all intensity. Furthermore, autoionization occurs only through the admixture of the $nd'[\frac{3}{2}]_1$ basis functions which are supposedly coupled to just a single continuum. Considering the simplicity of the model used and remembering that no adjustable parameters are employed, the agreement between Figs. 2 and 6 is indeed remarkable. The only major discrepancy is the absence of the ns' transitions in the simulation. The absence is the natural consequence of our setting the ns' transition moment and the ns' autoionization linewidths to zero; the zero-field experimental spectrum shows that this assumption is clearly not true.

Strictly speaking, we should revert to a multichannel approach in order to incorporate the ns' transitions into the simulation. In this work, we attempted a simpler approach. If we assume that a given eigenfunction of the Stark Hamiltonian contains a significant contribution from either the $ns'[\frac{1}{2}]_1$ or the $nd'[\frac{3}{2}]_1$ basis function, but not both, and that these two wave functions are coupled

to independent noninteracting continua, then we can write

$$\sigma(E) = \sum_{i=s,d} \sigma_0^i \cos^2\Delta^i \left[\sum_m q_m^i \tan\Delta_m^i - 1 \right]^2, \quad (17)$$

i.e., we simply add to the photoionization cross sections shown in Fig 6, the equivalent picture in which all intensity and linewidth is derived from the admixture of the $ns'[\frac{1}{2}]_1$ function. The result of such an approach is shown in Fig. 7; it can be seen that the ns' transitions are restored without significantly affecting the rest of the spectrum. This treatment is successful because the ns' states mix rather less than the nd' states with the other states, and they also have much less transition intensity and linewidth to contribute. It is noteworthy, however, that the ns' transitions in the simulated spectrum decrease in intensity with increasing electric field to a lesser extent than in the experimental spectrum. Our first major conclusion of the theoretical study is that our basic assumption regarding the importance of the $nd'[\frac{3}{2}]_1$ basis function in determining the intensities and linewidths is well justified, at least for the range of fields and energies in this simulation.

Figure 8 shows the simulated polarization dependence for the same part of the spectrum shown in Fig. 5, again using the two-continuum treatment Eq. (17). The simulation correctly predicts the qualitative differences between the $M=0$ and the $|M|=1$ spectra. The good agreement between experiment and theory allows us to identify with confidence the newly observed transitions by examining the calculated eigenfunctions. Thus for $M=0$ the one new series gaining intensity below 1000 V/cm is the $np'[\frac{1}{2}]_0$ component. This state does not exist for $|M|=1$ ($J\neq0$ for $|M|=1$), and we observe instead an unresolved combination of the other three components, $np'[\frac{1}{2}]_1$, $np'[\frac{3}{2}]_1$, and $np'[\frac{3}{2}]_2$. A second new series is also observed for $|M|=1$, but not $M=0$, which is identified by the calculations as an unresolved mixture of the $nd'[\frac{3}{2}]_2$ and $nd'[\frac{5}{2}]_2$ components. Note that in using these labels we are indicating the major contributor to states which are in reality strongly mixed and have no good quantum numbers except M.

The major differences between $M=0$ and $|M|=1$ arise from the selection rules given earlier (1) for the off-diagonal matrix elements of the Stark Hamiltonian. Of particular significance is the selection rule $\Delta J\neq0$ for
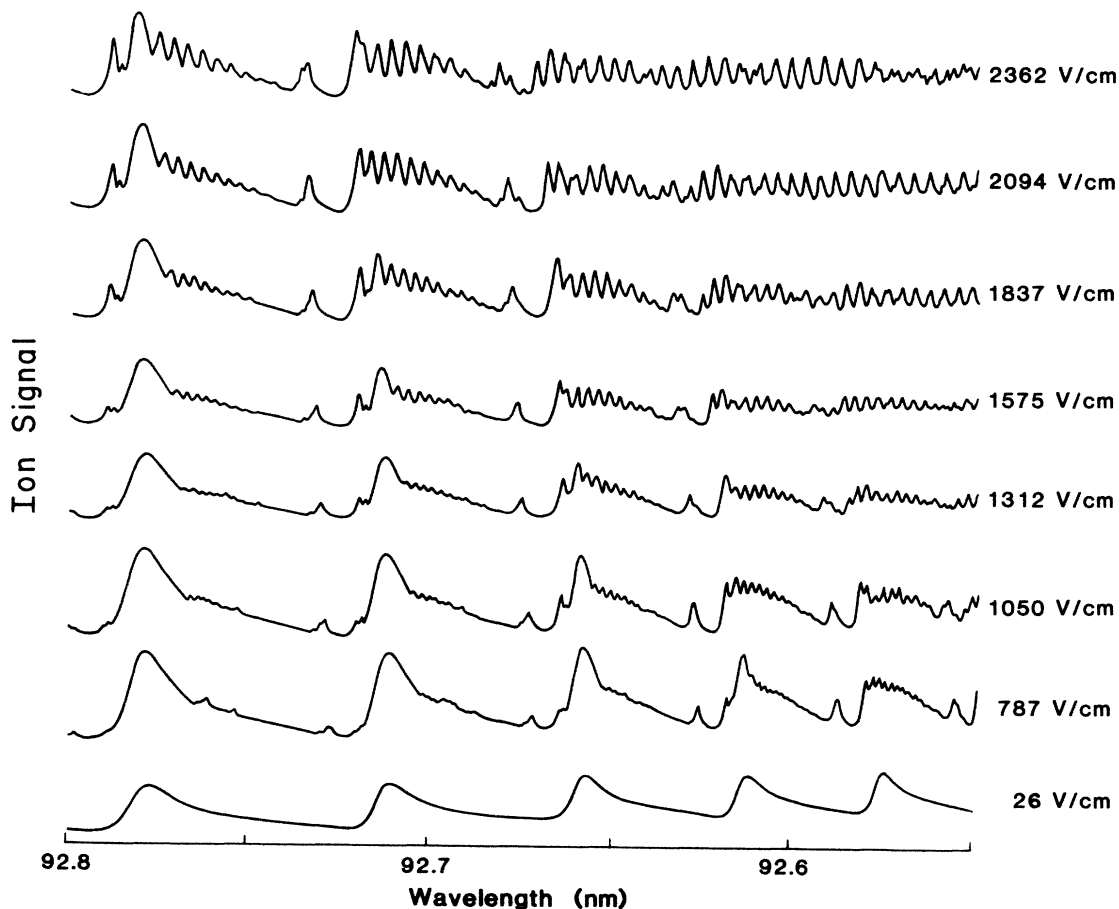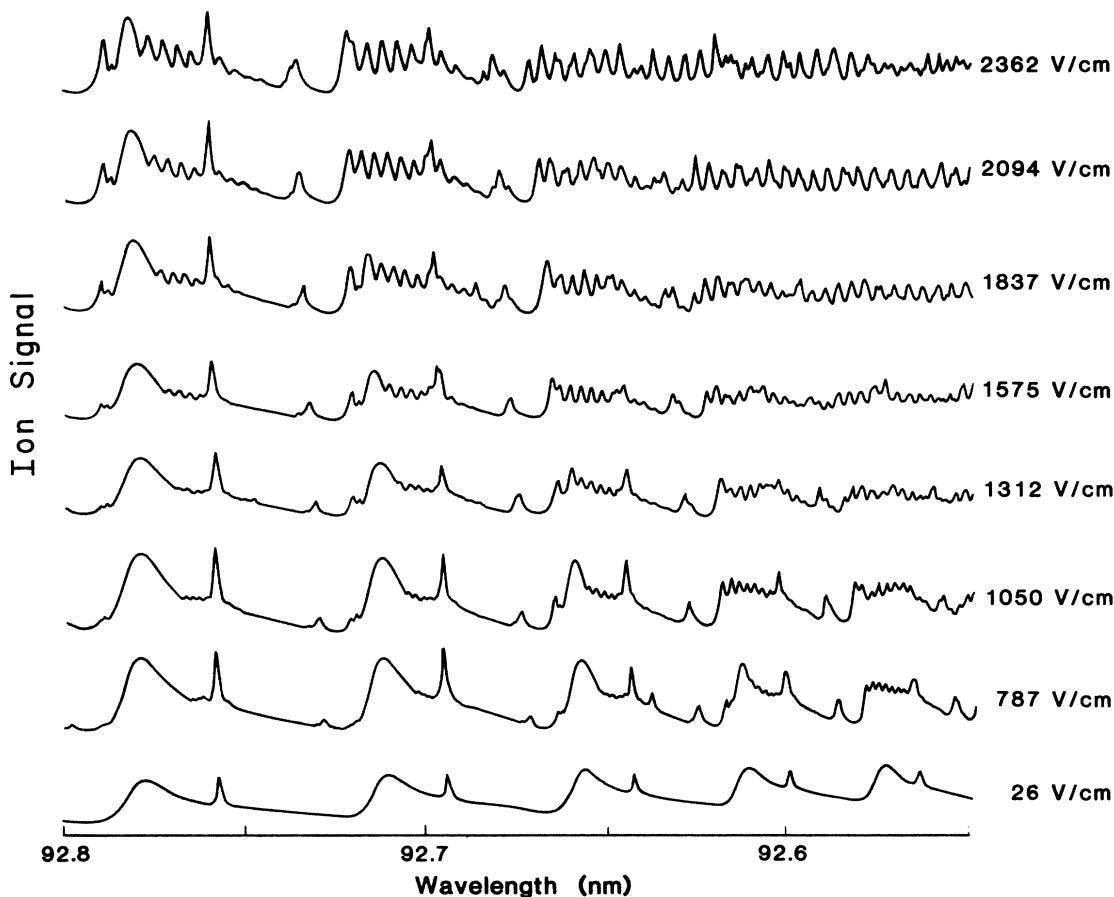

FIG. 6. Calculated Stark spectrum of Xe autoionizing Rydberg states for excitation into states with $|M|=1$. Electric field strengths and wavelength range as well as the scale are chosen to be the same as in Fig. 2. The ns' series is missing due to the procedure for calculating line intensities and widths (see text).

FIG. 7. Calculated Stark spectrum of Xe autoionizing Rydberg states for excitation into states with $|M| = 1$. Electric field strengths and wavelength range as well as the scale are chosen to be the same as in Figs. 2 and 6. All intensities and linewidths are assumed to arise from mixing with either the $ns'[\frac{1}{2}]$ or the $nd'[\frac{3}{2}]$ basis function but not both; it is also assumed that these basis functions couple independently to noninteracting continua (see text).
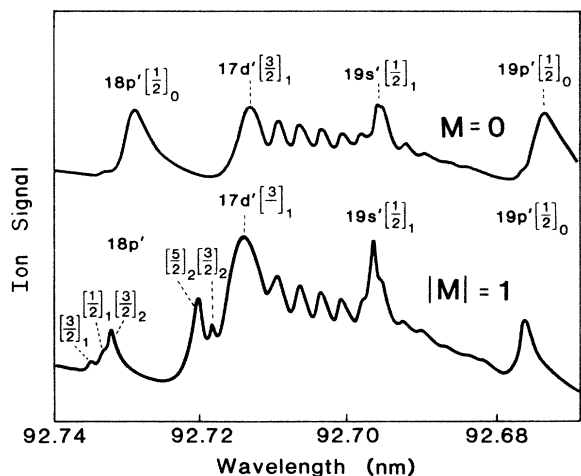

FIG. 8. Part of the calculated Stark spectrum for excitation into states with $M = 0$ (upper trace) and $|M| = 1$ (lower trace). The electric field strength $E = 1575$ V/cm and the wavelength range are the same as in Fig. 4. The lines are labeled using the assignment of the zero-field state contributing the main intensity.

$M = 0$ which does not apply to $|M| = 1$ Hence for $M = 0$ the $J = 1$ components of the np' series do not mix with the $nd'[\frac{3}{2}]_1$ wave function and hence these do not appear in the $M = 0$ spectrum. This selection rule also explains the absence of the nd' $J = 2$ components in the $M = 0$ spectrum. In the $|M| = 1$ set, a second-order coupling to the nd' $J = 1$ state occurs through the np' $J = 1$ or 2 states giving rise to the necessary intensity borrowing; for example, $nd'[\frac{3}{2}]_2$ couples to $np'[\frac{3}{2}]_2$ which couples to $nd'[\frac{3}{2}]_1$. The $\Delta J \neq 0$ selection rule prohibits this coupling for $M = 0$. The lack of $\Delta J = 0$ coupling for $M = 0$ means that the $\Delta J = \pm 1$ coupling is more effective; the $nd'[\frac{3}{2}]_1$ state couples more strongly with the $nf'[\frac{5}{2}]_2$ state for $M = 0$, explaining why the nd' lines merge into the manifold more quickly than for $|M| = 1$; see Sec. III C.

In Fig. 9 we plot a simulated Stark map, equivalent to that shown in Fig. 3. Note that good agreement is found concerning the manifold splitting and the shift of the nl' lines for $l' < 3$. An interesting question is whether the calculated manifold splittings show the same $n^{0.7}$ dependence as suggested by Delsart and Keller[12] as shown in
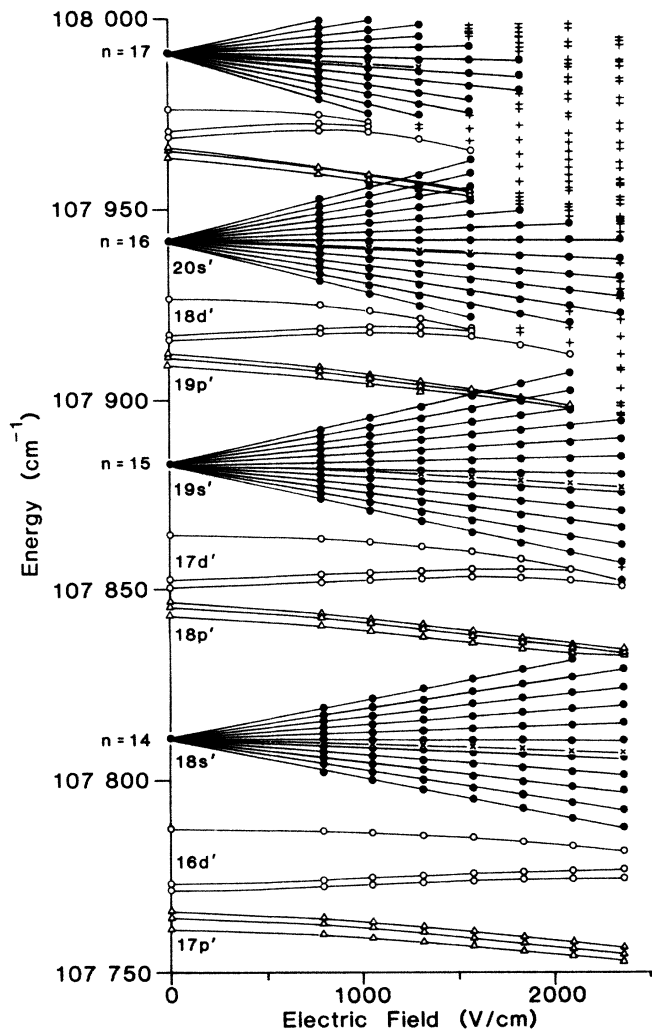
FIG. 9. Calculated Stark map for $|M| = 1$ in the region between the $n = 14$ and $n = 17$ manifolds. The symbols are the same as in Fig. 3; strongly mixed levels are marked by $+$.

FIG. 10. Plot of the calculated spacing between members of the Stark manifolds vs n with logarithmic scales as in Fig. 4 for various electric field strengths. The slope of each straight line is indicated.

Fig. 4. The log-log plot is shown in Fig. 10. The calculated points do not fit very well onto a straight line. The straight lines drawn through the points do have gradients in the range 0.7–0.87 with a tendency for the gradients to increase with increasing field. As a result it would seem that the $n^{0.7}$ law may not be a true representation of the dependence of the splittings; there does not appear to be
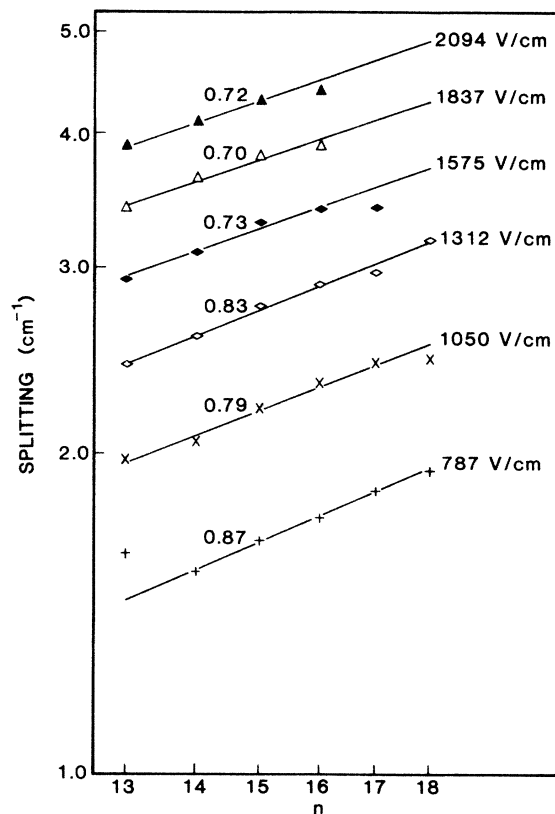
any theoretical justification for such a law in the case of xenon, while the experimental accuracy is insufficient to lead to any real conclusions.

Measured and calculated manifold splittings for $n = 14$ and 16 are compared in Table IV and agree well with each other. Calculated splittings for hydrogen are included in the table. For low n the manifolds show a larger splitting for Xe than for H, whereas for higher n the Xe values come closer to the H values.

We show in Fig. 11 what one could expect from improving our xuv linewidth of 1.2 to 0.2 cm^{-1}. The convolution of the calculated spectrum with a 0.2-cm^{-1} instrumental linewidth rather than 1.2 cm^{-1} indicates that

TABLE IV. Manifold splittings (cm^{-1}) for various electric field strengths from Xe measurements (Meas.) and calculations (Calc.). The values are compared with the calculated splittings in hydrogen.

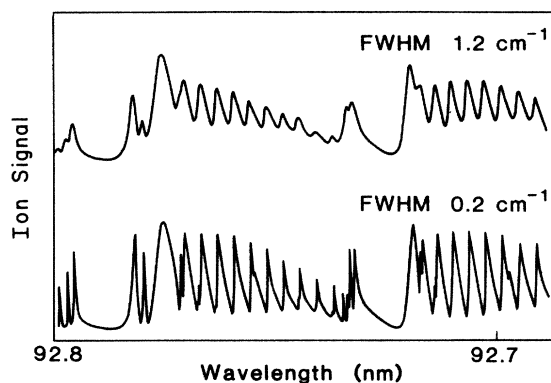| E (V/cm)	n = 14 Xe Meas.	n = 14 Xe Calc.	n = 14 H Calc.	n = 16 Xe Meas.	n = 16 Xe Calc.	n = 16 H Calc.
1312	2.51	2.57	2.35	2.73	2.88	2.69
1575	3.06	3.08	2.82	3.20	3.38	3.23
1837	3.57	3.60	3.29	3.84	3.87	3.76
2094	4.10	4.08	3.76	4.35	4.36	4.30
2362	4.59	4.62	4.23	4.68	4.77	4.84

FIG. 11. Plot of the calculated Stark spectrum for $E = 2362$ V/cm in the wavelength range 92.8–92.7 nm, convoluted with an instrumental linewidth of 1.2 cm^{-1} (upper trace) and 0.2 cm^{-1} (lower trace).

this would allow for a more stringent test of the model by showing the splittings in the p', d' complexes in more detail as well as the perturbations.

Finally, we note that our simple model cannot account for the oscillations, referred to in Sec. III D, which are superimposed on the $|M| = 1$ spectra between 1000 and 2000 V/cm. In addition, it becomes difficult to see a direct correlation between the simulated spectrum and the experimental spectrum for the highest electric fields and principal quantum numbers. This latter difficulty may simply be a basis-set truncation problem. Clearly a more rigorous theoretical treatment will be necessary in order to understand these features and it is hoped that MQDT calculations will be carried out in the near future for this system.

In conclusion, a simple model allows us to identify many of the features observed in the Stark spectrum and to understand the primary autoionization and intensity mechanisms. The lack of explanation for the oscillations points to the need for further theoretical work. At the same time, the simulated spectrum using an instrumental linewidth of 0.2 cm^{-1} suggests that additional experimental work would also be of great value.

ACKNOWLEDGMENTS

*Present address: Institut für Molekülphysik, Freie Universität Berlin, Arnimallee 14, D-1000 Berlin 33, West Germany.

†Present address: University Chemical Laboratory, Lensfield Road, Cambridge CB2 1EW, United Kingdom.

[1]H. Beutler, Z. Phys. **93**, 177 (1935).

[2]K. Yoshino and D. E. Freeman, J. Opt. Soc. Am. B **2**, 1268 (1985).

[3]K. T. Lu, Phys. Rev. A **4**, 579 (1971).

[4]R. F. Stebbings, C. J. Latimer, W. P. West, F. B. Dunning, and T. B. Cook, Phys. Rev. A **12**, 1453 (1975).

[5]J. P. Grandin and X. Husson, J. Phys. B **14**, 433 (1981).

[6]R. D. Knight and Liang-guo Wang, J. Opt. Soc. Am. B **2**, 1084 (1985).

[7]Liang-guo Wang and R. D. Knight, Phys. Rev. A **34**, 3902 (1986).

[8]R. D. Knight and Liang-guo Wang, J. Opt. Soc. Am. B **3**, 1673 (1986).

[9]*Laser Techniques in the Extreme Ultraviolet* (Boulder, Colorado, 1984), Proceedings of the Second Topical Meeting on Laser Techiques in the Extreme Ultraviolet, AIP Conf. Proc. No. 119, edited by S. E. Harris and T. B. Lucatorto (AIP, New York, 1984).

[10]K. D. Bonin, T. J. McIllrath, and K. Yoshino, J. Opt. Soc. Am. B **2**, 1275 (1985).

[11]B. E. Cole, J. W. Cooper, D. L. Ederer, G. Mehlman, and E. B. Saloman, J. Phys. B **13**, L175 (1980).

[12]C. Delsart and J. C. Keller, Phys. Rev. A **28**, 845 (1983).

[13]R. D. Knight and Liang-guo Wang, Phys. Rev. A **32**, 896 (1985).

[14]R. D. Knight and Liang-guo Wang, Phys. Rev. A **32**, 2751 (1985).

[15]A. H. Kung, Opt. Lett. **8**, 24 (1983); C. T. Rettner, E. E. Marinero, R. N. Zare, and A. H. Kung, J. Phys. Chem. **88**, 4459 (1984).

[16]T. P. Softley, W. E. Ernst, L. M. Tashiro, and R. N. Zare, Chem. Phys. **116**, 299 (1987).

[17]R. W. Falcone and J. Bokor, Opt. Lett. **8**, 1 (1983).

[18]M. L. Zimmerman, M. G. Littman, M. M. Kash, and D. Kleppner, Phys. Rev. A **20**, 2251 (1979).

[19]R. R. Freeman and N. P. Economou, Phys. Rev. A **20**, 2356 (1979).

[20]W. Sander, K. A. Safinya, and T. F. Gallagher, Phys. Rev. A **23**, 2448 (1981).

[21]W. L. Glab, G. B. Hillard, and M. H. Nayfeh, Phys. Rev. A **28**, 3682 (1983).

[22]D. A. Harmin, Phys. Rev. A **24**, 2491 (1981).

[23]D. A. Harmin, Phys. Rev. A **26**, 2656 (1982).

[24]D. A. Harmin, Phys. Rev. A **30**, 2413 (1984).

[25]K. Sakimoto, J. Phys. B **19**, 3011 (1986).

[26]D. E. Kelleher, in *Spectral Line Shapes V*, edited by B. Wende (de Gruyter, Berlin, 1981), p. 281.

[27]U. Fano, Phys. Rev. **124**, 1866 (1961).
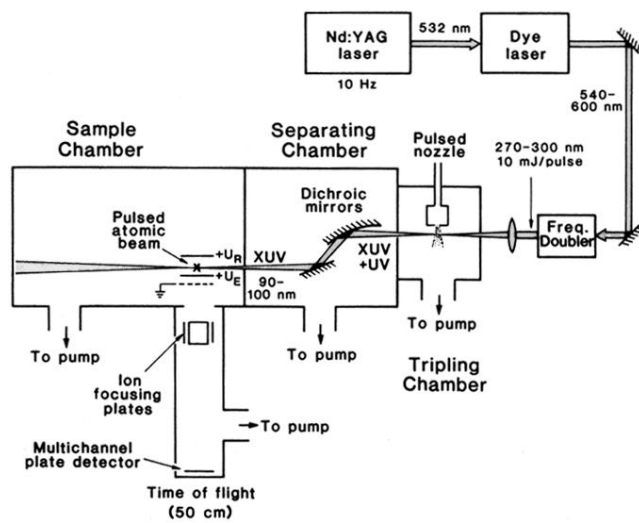
[28]A. R. Edmonds, J. Picart, N. Tran Minh, and R. Pullen, J. Phys. B **12**, 2781 (1979).

FIG. 1. Experimental setup.